Individual muscle segmentation in MR images: A 3D propagation through 2D non-linear registration approaches

Augustin C. Ogier, Michael Sdika, Alexandre Fouré, Arnaud Le Troter, David Bendahan

Individual muscle segmentation in MR Images: a 3D propagation through 2D non-linear registration approaches

Augustin Ogier[1], Michael Sdika[2], Alexandre Fouré[1], Arnaud Le Troter[1] and David Bendahan[1]

***Abstract*— Manual and automated segmentation of individual muscles in magnetic resonance images have been recognized as challenging given the high variability of shapes between muscles and subjects and the discontinuity or lack of visible boundaries between muscles. In the present study, we proposed an original algorithm allowing a semi-automatic transversal propagation of manually-drawn masks. Our strategy was based on several ascending and descending non-linear registration approaches which is similar to the estimation of a Lagrangian trajectory applied to manual masks. Using several manually-segmented slices, we have evaluated our algorithm on the four muscles of the quadriceps femoris group. We mainly showed that our 3D propagated segmentation was very accurate with an averaged Dice similarity coefficient value higher than 0.91 for the minimal manual input of only two manually-segmented slices.**

I. Introduction

Quantification of individual muscle volume is of high interest in the field of neuromuscular disorders for which muscle disease is associated with a loss of muscle tissue and a replacement by fat and in sport in which it is of interest to follow muscle volume changes resulting from repeated training sessions. The corresponding segmentation of muscle(s) in MR images has been recognized as challenging given the high variability of shapes and relative positions between muscles and among individuals. Also, the hardly discernible texture differences between individual muscles and the potential fatty infiltration of muscles in patients with neuromuscular disorders represent additional challenging factors. Besides these anatomical differences, subtle changes regarding the angular and relative position of individual muscles in MR images can generate other uncontrolled variability factors. So far, manual segmentation of anatomical structures has been used in multiple studies, and this approach has been widely acknowledged as time-consuming and operator-dependent [1].

More recently, several semi-automated / automated methods have been assayed on MR images. A random walk algorithm based on graphs has been reported by Baudin et al. [2] while Gilles et al. [3] proposed a method based on mesh deformable registration models. In order to take into account the large interindividual variability, Prescott et al. [4] used a semi-automatic segmentation method based on the preselection of appropriate templates selected from a database. On the basis of a combination of manual segmentation atlas-based registration, Ahmad et al. [5] proposed a semi-automatic segmentation tool for quadriceps muscles.

Overall, although of interest, these multi-atlas based methods have been mainly used for measurements of large muscle volumes. Sdika et al. [6] recently demonstrated the reliability of a multi-atlas segmentation approach for the automatic segmentation and volume quantification of individual leg muscles in rat. Le Troter et al. [7] evaluated the potential of this approach for quantification of individual muscle volume and reported the corresponding utilization for longitudinal studies in human. They illustrated that a fully-automated method was appropriate for large muscle groups but not for individual muscles and proposed a single-atlas based method as an alternative solution.

The purpose of the present study was to propose and characterize a new approach of semi-automated segmentation of individual muscles using a combination of 3D propagation and 2D registration of masks related to regions of interest.

II. SEGMENTATION PROPAGATION

Our method is semi-automatic since it requires manual segmentation of, at least, the two slices (2D) located on the inferior and superior bounds of the region of interest (3D).

A. Non-linear registration approaches

We used the *a priori* knowledge considering muscles as cylinders which can be nonlinearly distorded. We initially considered two naive methods with the aim of extrapolating the manual anatomical input in a few slices to the overall dataset within the region of interest. The first and second approaches considered an interpolation and a propagation method respectively. We also tested a third method corresponding to a mixture of the first two.

For the interpolation approach, we initially estimated the registration between the inferior and superior manual segmentations (i.e. masks) of the region of interest. Then we applied a linear interpolation between the resulting transformation and the identity in order to generate an automatic segmentation of the intermediate slices.

The propagation approach was iterative and consisted in two steps. Initially, successive registrations of each grey level of a given slice (considered as the source image) to the following slice (considered as the target image) were performed. The resulting transformations were then combined and used to generate the mask of each slice from one of the slice manually segmented.

[1]Augustin Ogier, Alexandre Fouré, Arnaud Le Troter and David Bendahan are with Aix Marseille Univ, CNRS, CRMBM, Marseille, France augustin.ogier@gmail.com

[2]Michael Sdika is with Univ.Lyon, INSA-Lyon, Université Claude Bernard Lyon 1, UJM-Saint Etienne, CNRS, Inserm, CREATIS UMR 5220, U1206, F-69XXX, LYON, France

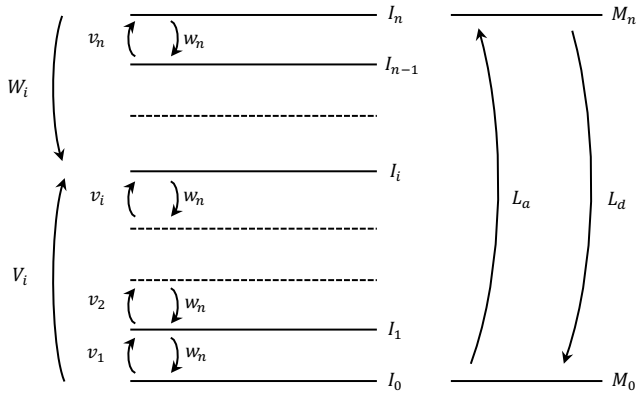

Fig. 1. Schematic representation of all transformations resulting from registration processes. M_i represent the manual masks and I_i the grey level MRI slices.

Given the similarities between our both approaches and the usual mathematical representations of flow in fluid mechanics [8], we chose to respectively define the interpolation approach as Lagrangian and the propagation approach as Eulerian, both terms used in the context of fluid registration [9], [10].

For both Lagrangian and Eulerian approaches, we tested ascending and descending versions (respectively denoted L_a, L_d, V_i, W_i, and illustrated in Fig.1). All registrations were estimated with the ANTs library through the command antsRegistration using the SyN transformation model [11]. For the Lagrangian approach, a cross-correlation metric was used for each label of the manual masks. One single cross-correlation metric between source and target grey level images was used for the Eulerian approach.

The Lagrangian approach did not take into account local anatomical deformations between the two manually segmented slices and considered anatomical variations as rather linear in the direction of propagation. The Eulerian approaches did follow anatomical variations but rapidly diverged given that errors were accumulating with the number of iterations and the accuracy decreased with respect to the distance from the starting slice. In contrast, the Lagrangian approaches did not follow the anatomy and was stable as it was driven by the segmentation of the final slice.

B. Our transformation merging method

Considering the properties of the four native approaches L_a, L_d, V_i, W_i, we chose to merge the resulting fields in order to keep the positive contributions only and implement a an original approach combining the straight attachment to the anatomical information of the Eulerian propagation and the convergence of the Lagrangian approach towards the target slice. The fusion of the fields resulting from the native approaches was obtained from the solution of the following optimization problem:

$$argmin(\alpha_i \|B_i - v_i \circ B_{i-1}\|^2 + \beta_i \|B_i - W_i \circ L_a\|^2) \qquad (1)$$

where i is the index of the current slice to obtain, B_i the resulting fields (i.e. the solution of the minimization), v_i the Eulerian ascending displacement field relative to the slice i, W_i the composition of Eulerian descending displacement fields from n to i, L_a the Lagrangian displacement field which allowed to use the Eulerian descending displacement field in this privileged ascending version, and finally the coefficients α_i, β_i which allowed to determine the contribution of each term in equation 1. The solution of B_i is given by the following equation 2:

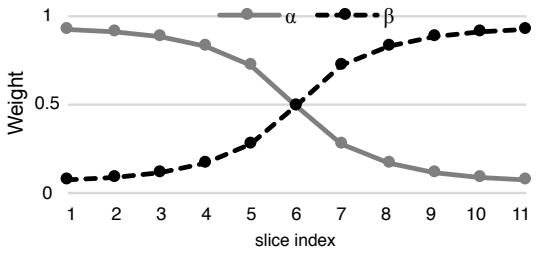

Fig. 2. Representation of weighting coefficients values α_i, β_i for each slice i to be interpolated

$$B_i = \alpha_i(v_i \circ B_{i-1}) + \beta_i(W_i \circ L_a) \qquad (2)$$

The determination of coefficients α_i, β_i illustrated in Fig 2 was based on the assumption of a reduced accuracy of the Eulerian propagation with respect to the distance from the starting slice. This process can be repeated for a version with an emphasis on the descending approaches (See Algorithm 1, more specifically the term A_i). Then, both resulting fields B_i and A_i were merged into a single field P_i which was applied to the mask M_0 in order to obtain each mask M_i (2D) with the aim of getting the segmentation of the whole region of interest (3D). More details about our method are described in Algorithm 1.

Algorithm 1 segmentation propagation

Require: I (MRI images)
M (Manual mask only 2 slices: M_0, M_n)
Ensure: M (Full segmented mask)
$L_a = \text{SyN}(M_0, M_n)$
$L_d = \text{SyN}(M_n, M_0)$
$V_{-1} \leftarrow W_{n+1} \leftarrow Identity$
for i $\leftarrow$ 0 **to** n **do**
$v_i = \text{SyN}(I_i, I_{i+1})$
$V_i = v_i \circ V_{i-1}$
$w_{n-i} = \text{SyN}(I_{n-i}, I_{n-i-1})$
$W_{n-i} = w_{n-i} \circ W_{n-i+1}$
end for
for i $\leftarrow$ 0 **to** n **do**
$B_i = \alpha_i(v_i \circ P_{i-1}) + \beta_i(W_i \circ L_a)$
$A_{n-i} = \beta_{n-i}(w_{n-i} \circ A_{n-i+1}) + \alpha_{n-i}(V_{n-i} \circ L_d)$
end for
for i $\leftarrow$ 0 **to** n **do**
$P_i = \alpha_i B_i + \beta_i(A_i \circ L_a)$
$M_i = P_i(M_0)$
end for
return M

Our method allowed to keep the high accuracy of each Eulerian propagation approach near their respective initial slice (i.e. the lower slice of the field of interest for the ascending version and the upper slice for the descending version). The deformation fields resulting from the registration between the masks manually segmented used for the Lagrangian approach were used in order to perform a reference frame shift and merge both Eulerian approaches.

III. EXPERIMENTAL VALIDATION

A. Subjects

The right thigh of 25 healthy men (22 $\pm$ 1 years, height 178 $\pm$ 6 cm, weight 68 $\pm$ 7 kg) were imaged using a 1.5T MRI scanner (MAGNETOM Avanto, Siemens AG, Healthcare Sector, Erlangen, Germany). T_1-weighted high-resolution images (13 slices, field of view = 220 mm x 220 mm; matrix = 576 x 576; time repetition = 549 ms; echo time = 13 ms; number of repetitions = 1; slice thickness = 6 mm; gap between slices = 6 mm, acquisition time = 5 min 18 s) were recorded using a turbo spin echo sequence. The most distal slice was always acquired at approximately 10 cm upper the proximal border of the patella. The study was approved by the local human research committee and was conducted in conformity with the Declaration of Helsinki.

The manual segmentation of each individual muscle of the *quadriceps femoris* (QF), i.e. *vastus lateralis* (VL), *rectus femoris* (RF), *vastus medialis* (VM) and *vastus intermedius* (VI), on all slices was performed by an expert (A.F., with 7 years of experience in evaluation of muscle anatomy and geometry) using FSLview software, the 3D viewer included in the FSL toolbox [12]. These manual segmentations were considered as ground truth and were used in the following sections for the comparative analysis with our propagated segmentation.

B. Comparison of our method with native Eulerian and Lagrangian approaches

The DICE similarity coefficient (DSC [13]) obtained for each slice are illustrated in Fig.3 for our rectified propagation approach (P) and the four native approaches L_a, L_d, V_i, W_i. These results highlighted our initial assumptions regarding that both DSC values of ascending and descending Eulerian approaches (respectively V_i and W_i) were optimal for their respective initial slice but decreased exponentially for the other slices. DSC values of ascending and descending Lagrangian approaches (respectively L_a and L_d) were similar and the small differences between the results were mainly due to registration errors. The results associated to L_a and L_d showed that these approaches, on the contrary to V_i and W_i, were less accurate for intermediate slices but converged efficiently for their respective final slice.

The results indicated in Fig. 3 clearly illustrated that our propagation approach did not only keep the positive contributions of each native approach but also resulted in a more accurate segmentation for each intermediate slice.

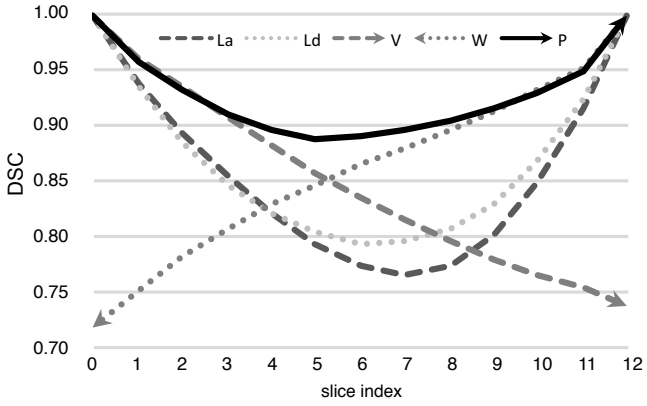

Fig. 3. DSC values evolution for each slice comparing each method

C. Qualitative and Quantitative validation

The DSC, the false negative volume fraction (FNVF), the false positive volume fraction (FPVF) and the muscle volume similarity fraction (MVSF) were used to estimate the performance of our method considering manual segmentation as the ground-truth (all ranged from 0 to 1).

Values from Table.1 are presented as mean $\pm$ SD. These metrics were obtained from a comparative analysis between our propagation method based on an initial manual input of two slices (located on the inferior and superior bounds of the region of interest) and the overall manual segmentation. As indicated, the average DSC values ranged from 0.87 to 0.94 while the FNVF and the FPVF values ranged from 0.04 to 0.18 and 0.07 to 0.10 respectively. Regarding the performance related to the volume measurements, i.e. MVSF, the range was 0.03-0.13. It is noteworthy that the segmentation of the VM was the less accurate. As can be seen in Fig. 4, VM is the individual muscle with the larger anatomical variability in the axial plane.

TABLE I
METRICS FOR EACH MUSCLE OF THE *quadriceps femoris*

muscle	DSC	FNVF	FPVF	MVSF
VL	0.94±0.01	0.04±0.01	0.08±0.02	0.05±0,03
RF	0.90±0.03	0.10±0.03	0.10±0.04	0.03±0,02
VM	0.87±0.02	0.18±0.03	0.07±0.02	0.13±0,05
VI	0.93±0.01	0.06±0.02	0.08±0.03	0.04±0,04

IV. CONCLUSION

So far, very few segmentation tools have been described for individual muscles and their corresponding accuracy was variable. In many other studies, segmentation has been performed manually and has been recognized as time consuming and operator-dependent. In the present study, we proposed a supervised method which provides a high segmentation accuracy with a minimal amount of time devoted to manual segmentation and a low computational expense. Using a manual input of 2 slices, the time allocated to manual segmentation can be reduced by 85%.

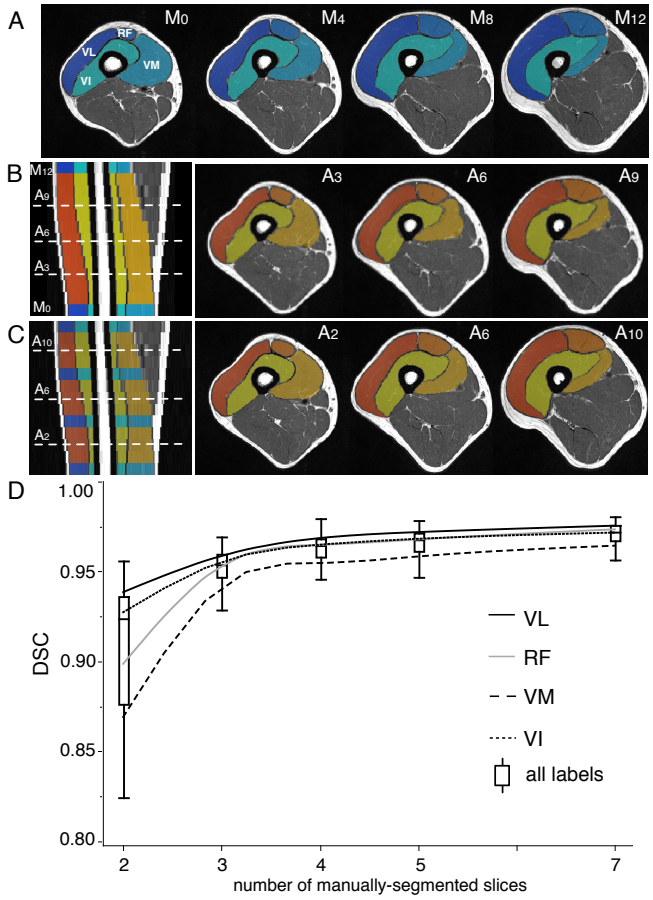

Fig. 4. A: Axial views of four manually-segmented slices M_0, M_4, M_8, M_{12}, B: Sagittal and axial views of three intermediate slices A_3, A_6, A_9 automatically-segmented slices using M_0, M_{12} masks, C: Sagittal and axial views of three intermediate slices A_2, A_6, A_{10} automatically-segmented slices using M_0, M_4, M_8, M_{12} masks, D: Boxplot representation of the relationship between DSC values and the number of manually-segmented slices

The accuracy of our method was determined by various parameters such as the anatomy of the areas of interest, their variability in the axial plane and the distance between the slices manually segmented. We mainly showed that with the initial input of only two manually segmented slices, the automated segmentation of the QF muscles was accurate on a large part of the thigh. According to the metrics reported in Table 1, our method provided better results as compared to the full multi-atlas based automatic approach Le Troter et al. initially proposed for the same muscle group [7] with average DSC values ranging from 0.72 to 0.94. We expect an even better accuracy of our method using a larger amount of manually-segmented slices as initial input. As illustrated in Fig. 4D, an initial input of 3, 4, 5 and 7 slices manually-segmented at regular intervals, led to a substantial increase in the mean DSC values for the individual and whole set of labels. This increase was likely due to the additional information provided by the additional manually-segmented slices.

Given that the anatomy of whole leg muscles is quite similar to the anatomy of the QF muscles, we expect that our approach will also be robust for other individual muscles of the thigh or calf inasmuch as our method can be adapted to anatomical variations using the coefficients. On the same basis, the segmentation of fatty-infiltrated muscles in patients with neuromuscular disorders or other diseases resulting in muscle volume loss and/or fatty infiltration might also be possible. This will have to be tested in the near future.

REFERENCES

[1] Y. Barnouin, G. Butler-Browne, T. Voit, D. Reversat, N. Azzabou, G. Leroux, A. Behin, J. S. McPhee, P. G. Carlier, and J.Y. Hogrel, "Manual segmentation of individual muscles of the quadriceps femoris using MRI: a reappraisal," *Journal of magnetic resonance imaging: JMRI*, vol. 40, no. 1, pp. 239–247, July 2014.

[2] P. Y. Baudin, N. Azzabou, P. G. Carlier, and N. Paragios, "Automatic skeletal muscle segmentation through random walks and graph-based seed placement," in *International Symposium Biomedical Imaging (ISBI)*, Barcelone, Spain, May 2012, pp. 1036–1039.

[3] B. Gilles, L. Moccozet, and N. Magnenat-Thalmann, "Anatomical modelling of the musculoskeletal system from MRI," *International Conference on Medical Image Computing and Computer-Assisted Intervention*, vol. 9, no. Pt 1, pp. 289–296, 2006.

[4] J. W. Prescott, T. M. Best, M. S. Swanson, F. Haq, R. D. Jackson, and M. N. Gurcan, "Anatomically Anchored Template-Based Level Set Segmentation: Application to Quadriceps Muscles in MR Images from the Osteoarthritis Initiative," *Journal of Digital Imaging*, vol. 24, no. 1, pp. 28–43, Feb. 2011.

[5] E. Ahmad, M. H. Yap, H. Degens, and J. S. McPhee, "Atlas-registration based image segmentation of mri human thigh muscles in 3d space," in *Proc. SPIE*, 2014, vol. 9037, pp. 90371L–90371L–12.

[6] M. Sdika, A. Tonson, Y. Le Fur, P. J. Cozzone, and D. Bendahan, "Multi-atlas-based fully automatic segmentation of individual muscles in rat leg," *Magma (New York, N.Y.)*, vol. 29, no. 2, pp. 223–235, Apr. 2016.

[7] A. Le Troter, A. Foure, M. Guye, S. Confort-Gouny, J. P. Mattei, J. Gondin, E. Salort-Campana, and D. Bendahan, "Volume measurements of individual muscles in human quadriceps femoris using atlas-based segmentation approaches," *Magma (New York, N.Y.)*, vol. 29, no. 2, pp. 245–257, Apr. 2016.

[8] J. Donea, A. Huerta, J. Ph. Ponthot, and A. Rodriguez-Ferran, "Arbitrary Lagrangian-Eulerian Methods," in *Encyclopedia of Computational Mechanics*. John Wiley & Sons, Ltd, Chichester, UK, Nov. 2004.

[9] B. B. Avants, P. T. Schoenemann, and J. C. Gee, "Lagrangian frame diffeomorphic image registration: Morphometric comparison of human and chimpanzee cortex," *Medical Image Analysis*, vol. 10, no. 3, pp. 397–412, June 2006.

[10] C. Brun, N. Lepore, X. Pennec, Yi-Yu Chou, A. D. Lee, M. Barysheva, G. I. de Zubicaray, K. L. McMahon, M. J. Wright, A. W. Toga, and P. M. Thompson, "A lagrangian formulation for statistical fluid registration," in *2009 IEEE International Symposium on Biomedical Imaging: From Nano to Macro*, June 2009, pp. 975–978.

[11] B. B. Avants, C. L. Epstein, M. Grossman, and J. C. Gee, "Symmetric diffeomorphic image registration with cross-correlation: evaluating automated labeling of elderly and neurodegenerative brain," *Medical Image Analysis*, vol. 12, no. 1, pp. 26–41, Feb. 2008.

[12] M. Jenkinson, C. F. Beckmann, T. E. J. Behrens, M. W. Woolrich, and S. M. Smith, "FSL," *NeuroImage*, vol. 62, no. 2, pp. 782–790, Aug. 2012.

[13] J. K. Udupa, V. R. Leblanc, Y. Zhuge, C. Imielinska, H. Schmidt, L. M. Currie, B. E. Hirsch, and J. Woodburn, "A framework for evaluating image segmentation algorithms," *Computerized Medical Imaging and Graphics: The Official Journal of the Computerized Medical Imaging Society*, vol. 30, no. 2, pp. 75–87, Mar. 2006.